CONTINUOUS WAVE LASER EXCITED ATOMIC AND MOLECULAR FLUORESCENCE

By

MARLANA BETH BLACKBURN

A DISSERTATION PRESENTED TO THE GRADUATE COUNCIL
OF THE UNIVERSITY OF FLORIDA
IN PARTIAL FULFILLMENT OF THE REQUIREMENTS FOR THE
DEGREE OF DOCTOR OF PHILOSOPHY

UNIVERSITY OF FLORIDA

1978

ACKNOWLEDGEMENTS

The author wishes to express her sincere appreciation to all members of the research group of Dr. J. D. Winefordner for their cooperation. In particular a special expression of gratitude must be made to Dr. Benjamin Smith for his experimental assistance and general encouragement.

Dr. J. D. Winefordner is a remarkable research director and human being. His patience and understanding made this author's graduate education very rewarding.

TABLE OF CONTENTS

page

ACKNOWLEDGEMENTS ii

ABSTRACT iv

CHAPTER

I. INTRODUCTION 1

II. SATURATED SODIUM FLUORESCENCE IN FLAMES 4
    Theory 6
    Experiment 23

III. MOLECULAR FLUORESCENCE IN FLAMES 39
    Experiment 40
    Conclusion 61

APPENDIX 63

REFERENCES 67

BIOGRAPHICAL SKETCH 70

Abstract of Dissertation Presented to the Graduate Council
of the University of Florida in Partial Fulfillment of
the Requirements for the Degree of Doctor of Philosophy

CONTINUOUS WAVE LASER EXCITED ATOMIC AND MOLECULAR FLUORESCENCE

By

Marlana Beth Blackburn

December 1978

Chairman: James D. Winefordner
Major Department: Chemistry

The tunable continuous wave (cw) dye laser is used to saturate the 589.6 nm transition of sodium in two flames of different efficiency. A quantum three level model is used to compare theoretical and experimental results. Plots of absolute fluorescence radiance vs. source irradiance are presented for source intensities varying over six orders of magnitude. The agreement between theory and experiment is quite good. The cw dye laser has also been used as an excitation source for molecular fluorescence. Fluorescence spectra of five species were recorded: SrOH, CaOH, CrO, MnO, and C_2. Differences in the fluorescence spectra as a function of excitation wavelength are investigated.

CHAPTER I
INTRODUCTION

Analytical atomic spectroscopy comprises three techniques: (i) atomic emission spectroscopy (AES); (ii) atomic absorption spectroscopy (AAS); and (iii) atomic fluorescence spectroscopy (AFS). All three involve the observation of electronic excitation and de-excitation processes in atoms. In the first technique, AES, the origin of the excitation energy is thermal or chemical; the atoms draw energy from the surroundings via collision or chemical reaction. In the last two methods, the atoms draw energy from light. This requires an external excitation source, an optical pump. Certain characteristics of this source can limit the practicality of AAS and AFS, e.g., atomic absorption measurements requiring high frequency and intensity stability.

Consider the evaluation of a continuous wave (cw) tunable dye laser for AFS. The ideal excitation source for atomic fluorescence would possess:

(i) narrow spectral bandwidth;
(ii) high peak power;
(iii) well defined beam characteristics; and
(iv) wavelength tunability over a wide range.

The spectral bandwidth of a cw dye laser is acceptable and may be decreased by use of an etalon, grating, or prism.

The "always-on" nature of this system mitigates against the attainment of high peak powers [peak power = (average power) (duty cycle)$^{-1}$]. However, this drawback can be overcome because the optical quality of a cw dye laser allows it to be focused to a very small spot, thereby producing a large source irradiance (W m^{-2}). The main failing of the cw dye laser as it exists today is its limited tunability range. The overwhelming number of analytically useful (i.e., resonance) transitions lie below 450 nm and extend into the ultraviolet (uv) region. The wavelength range of the cw dye laser is dependent on the optical pumping source and the availability of suitable dyes. With a 24 W Ar$^+$ laser pump, it is possible to generate lasing output of tens of milliwatts from 415 to 700 nm. (The electrical power requirements of such a pumping source are quite large, 440 V, 3 phase, 100 A. The large amount of heat to be dissipated also poses a problem.) The lower wavelength limit is determined by the shortest wavelength lasing Ar$^+$ transition available to pump a dye. There are two schemes for generating shorter wavelength lasing light: (i) pumping blue dyes with a uv source (e.g., a cw Kr$^+$ laser); and (ii) frequency doubling or mixing of visible radiation using nonlinear crystals. The first solution is limited by the dismal efficiency of the uv lasers and the dearth of dyes which can withstand uv irradiation. The alternative is more attractive but still suffers from heat dissipation problems and low crystal efficiency (≈ 1%). Maximum output powers of hundreds of microwatts at wavelengths down to 250 nm are attained (1). Thus the lack of tunable violet and uv radiation prevents the cw dye laser from approaching perfection, or even practicality, as an excitation source for atomic fluorescence.

There are several tasks, however, which this system may perform, and two of these form the subject of this work. Neither is strictly an analytical project. The first, an examination of sodium saturation in flames, compares the theoretical and experimental dependence of fluorescence radiance on source irradiance; the second is a presentation of fluorescence spectra of several molecular species.

CHAPTER II
SATURATED SODIUM FLUORESCENCE IN FLAMES

The possibility of saturating atomic and molecular transitions as a means of determining fundamental parameters in plasmas was first suggested by Measures (2). In his words, "A moderate laser, operating at a frequency that coincides with the frequency of an emission line can selectively excite a large number of the appropriate atoms into the upper state of the transition along the path of the laser beam. This will cause an intensification of the spontaneous emission . . . from the volume exposed to the laser radiation. If this enhanced emission can be identified from the background radiation emanating from the rest of the plasma, useful localized information about the state of the plasma can be ascertained" (2, p. 5232). Measures later investigated the atomic fluorescence of a potassium plasma when excited by a ruby laser (3). Workers pursuing Measures' suggestion have developed two experimental configurations: (i) a pulsed case, where the excitation radiation is applied during a short interval, and the fluorescence decay is monitored (4); and (ii) a steady-state case, where the excitation radiation is applied during an interval long enough to allow the fluorescence to reach some stable level (5). In either case, the plasma parameter determined is n_T, the total species concentration. The first approach has proved to be experimentally difficult since it requires the generation of stable, high powered short pulses and the detection of fast decay processes after the source is switched off. (Advances in state-of-the-art electronic devices, e.g., shutters, PM tubes, can remove these objections.) The steady-state approach is taken in this work and, indeed, has become the common technique.

The term "saturation" describes the leveling off (plateau) of the steady-state fluorescence signal as the source intensity is increased. It is an effect observed only at rather large source irradiances. In general, conventional (i.e., non-laser) sources cannot produce the high radiation fields necessary to saturate atomic and molecular transitions; they operate in the linear region, where the fluorescence signal is directly proportional to the source intensity. However, because many types of currently available lasers can reach and exceed the required "saturation" irradiances, the proposal of Measures has been applied to plasmas (and flames) by a number of workers using lasers as excitation sources. Omenetto et al. with a N_2 pumped dye laser investigated saturation effects for several different elements in analytically useful flames (6). De Olivares used a higher powered but similar system in an extremely detailed examination of flame saturation phenomena (7). Baronavski and McDonald measured C_2 concentrations in an oxyacetylene flame (8). Eckbreth et al. determined CH and CN concentrations in an oxyacetylene and nitrous oxide-acetylene flame, respectively (9). Kuhl et al. (10), Sharp and Goldwasser (11), Smith et al. (12), and Daily and Chan (13) have investigated sodium fluorescence under pulsed and cw excitation.

The $3^2S_{\frac{1}{2}} - 3^2P_{3/2,\frac{1}{2}}$ transitions of atomic sodium provide a fair approximation to a 2-level system and a good approximation to a 3-level system. Theoretical expressions (both 2- and 3-level) for Na type atoms have been developed to describe the fluorescence radiance vs. laser irradiance (14). The following derivation is taken from reference 14. Moreover, the wavelengths lie in the visible at the peak of an efficient (and cheap) laser dye, Rhodamine 6G. It is possible, therefore, to pump these transitions at large source powers and observe the fluorescence radiance while manipulating various experimental parameters. Following the derivation of the appropriate theoretical expressions, experimental results will be presented and discussed.

Theory

The atomic fluorescence radiance for any atom (2- or n-level) is given by (15):

$$B_{F_{\substack{j\to k\\ \ell\to m}}} = \left(\frac{\ell}{4\pi}\right) Y_{jk} E_{\nu_{\ell m}} \left(\frac{h\nu_{jk}}{c}\right) B_{\ell m} n_{\ell} \left[1 - \frac{g_{\ell}}{g_m}\frac{n_m}{n_{\ell}}\right] \tag{1}$$

where

$B_{F_{j\to k,\ \ell\to m}}$ = atomic fluorescence radiance for j→k radiative process and for ℓ→m radiative excitation process, J s^{-1} m^{-2} sr^{-1};

ℓ = fluorescence path length in direction of observation, m;

Y_{jk} = fluorescence quantum efficiency, photons fluoresced/photons absorbed, dimensionless;

$E_{\nu_{\ell m}}$ = spectral irradiance of continuum source at frequency $\nu_{\ell m}$ of excitation (ℓ is lower level from which transition begins and m is upper level at which the transition ends), J s^{-1} m^{-2} Hz^{-1};

$h\nu_{\ell m}$ = energy of exciting photon, J;

c = speed of light, m s^{-1};

$B_{\ell m}$ = Einstein coefficient of induced absorption, i.e., absorption transitions per spectral energy density per absorbing species, m^3 J^{-1} s^{-1} Hz;

n_ℓ = density (concentration) of species (absorbers) in lower level ℓ, m^{-3};

g_ℓ or m = statistical weights of ℓ or m levels, dimensionless; and

n_m = density (concentration) of upper level of excitation, m^{-3}.

The equation above was derived with the assumption of an unpolarized source and square beam geometry. In order to treat the more realistic case of circular beam geometry and to include polarization effects (a factor of ½), Equation 1 transforms to

$$B_{F_{\substack{j\to k\\ \ell\to m}}} = \left(\frac{r}{16}\right) Y_{jk}\, E_{\nu_{\ell m}} \left(\frac{h\nu_{jk}}{c}\right) B_{\ell m}\, n_\ell \left[1 - \frac{g_\ell}{g_m}\frac{n_m}{n_\ell}\right] \tag{2}$$

where r = excitation source radius, m.

The dependence of B_F on source intensity $E_{\nu_{\ell m}}$ is not clearly shown by Equation 2 since $E_{\nu_{\ell m}}$ also affects n_m/n_ℓ. To express B_F in terms of n_T, a constant for a given system, requires knowledge of the relationships between the populations of each level. For the purposes of this derivation, the following assumptions are made: (i) the system is characterized as an ensemble of atoms having only three energy levels, 1, 2, and 3, with statistical weights g_1, g_2, and g_3, respectively, and having populations n_1, n_2, and n_3, with $n_1 + n_2 + n_3 = n_T$; (ii) the atoms are present in thermodynamic equilibrium at low concentration so that self-absorption is not considered; (iii) the laser radiation does not affect the energy distribution of the atoms and the temperature T of the system; (iv) the atomic system is spatially homogeneous with respect to both concentration and temperature; (v) the excitation source is a spectral continuum; and finally (vi) steady-state conditions have been achieved. The sodium energy level diagram and various parameters are shown in Figure 1.

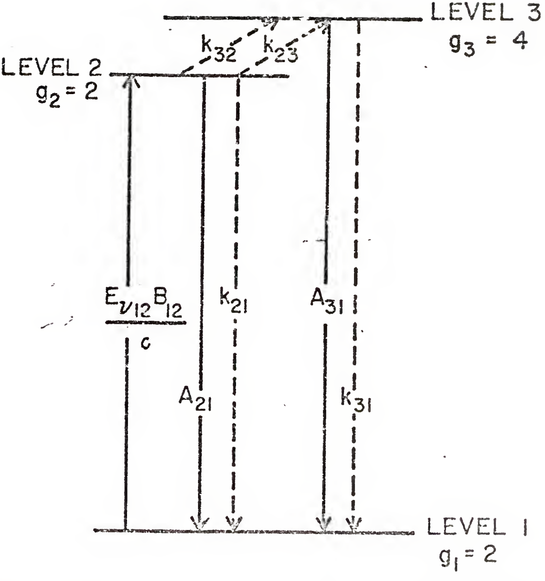

Figure 1. Energy level diagram for sodium doublet at 589 nm. Radiative processes of interest are denoted by solid lines, nonradiative processes by dashed lines.

The general expressions for the time rate of change of populations n_3 and n_2 are given by

$$\frac{dn_3}{dt} = -\left[\frac{B_{31}E_{\nu_{13}}}{c} + \frac{B_{32}E_{\nu_{23}}}{c} + A_{31} + A_{32} + k_{31} + k_{32}\right] n_3 + \left[\frac{B_{13}E_{\nu_{13}}}{c} + k_{13}\right] n_1 + \left[\frac{B_{23}E_{\nu_{23}}}{c} + k_{23}\right] n_2 \tag{3}$$

$$\frac{dn_2}{dt} = -\left[\frac{B_{23}E_{\nu_{23}}}{c} + \frac{B_{21}E_{\nu_{12}}}{c} + A_{21} + k_{21} + k_{23}\right] n_2 + \left[\frac{B_{32}E_{\nu_{23}}}{c} + A_{32} + k_{32}\right] n_3 + \left[\frac{B_{12}E_{\nu_{12}}}{c} + k_{12}\right] n_1 \tag{4}$$

where

A's = Einstein coefficient of spontaneous emission for optical transition indicated, s^{-1}; and

k's = pseudo first order rate constant for collisional process indicated, s^{-1}.

For Na type atoms, the two upper levels, 2 and 3, lie very close together and cannot exchange radiatively, i.e., $A_{32} = 0$. In addition, the thermal population of these levels is neglected, i.e., $k_{12} = k_{13} = 0$. After making these substitutions and considering the case of ν_{12} absorption and

and emission, i.e., $E_{\nu_{23}} = E_{\nu_{13}} = 0$, Equations 3 and 4 simplify to

$$\frac{dn_3}{dt} = -(A_{31} + k_{31} + k_{32})\, n_3 + k_{23}\, n_2 \qquad (5)$$

$$\frac{dn_2}{dt} = -[\frac{B_{21}E_{\nu_{12}}}{c} + A_{21} + k_{21} + k_{23}]\, n_2 + k_{32}\, n_3 + \frac{B_{12}E_{\nu_{12}}}{c}\, n_1 \qquad (6)$$

Setting Equation 5 equal to zero (steady state) and solving for n_3/n_2 gives

$$\frac{n_3}{n_2} = \frac{k_{23}}{A_{31} + k_{31} + k_{32}} \qquad (7)$$

Substituting for n_3 in terms of n_2 in Equation 6, setting the expression equal to zero, and solving for n_2/n_1 yields

$$\frac{n_2}{n_1} = \frac{\frac{B_{12}E_{\nu_{12}}}{c}}{\frac{B_{21}E_{\nu_{12}}}{c} + A_{21} + k_{21} + k_{23} - \frac{k_{32}\, k_{23}}{A_{31} + k_{31} + k_{32}}} \qquad (8)$$

and, continuing the procedure

$$\frac{n_3}{n_1} = \frac{\frac{B_{12}E_{\nu_{12}}}{c}\left(\frac{k_{23}}{A_{31} + k_{31} + k_{32}}\right)}{\frac{B_{21}E_{\nu_{12}}}{c} + A_{21} + k_{21} + k_{23}} \qquad (9)$$

The quantum efficiency Y_{21} is defined as the ratio of photons fluoresced to photons absorbed. It can also be expressed as a ratio of the rate of emission to the sum of all rates of deactivation. There are four pathways for appearance or disappearance of molecules from level 2. The absorber may emit (rate constant = A_{21}); it may collisionally deactivate to level 1 (k_{21}); it may collisionally cross to level 3 (k_{23}); and it may cross back to level 2 from level 3 ($-k_{32}$). The corresponding ratio is

$$Y_{21} = \frac{n_2\ A_{21}}{A_{21}\ n_2 + k_{21}\ n_2 + k_{23}\ n_2 - k_{32}\ n_3} \qquad (10)$$

Dividing through by n_2/n_2

$$Y_{21} = \frac{A_{21}}{A_{21} + k_{21} + k_{23} - \frac{n_3}{n_2} k_{32}} \qquad (11)$$

Substituting from Equation 7 for n_3/n_2 yields

$$Y_{21} = \frac{A_{21}}{(A_{21} + k_{21} + k_{23})\ [1 - \frac{k_{32}\ k_{23}}{(A_{21} + k_{21} + k_{23})(A_{31} + k_{31} + k_{32})}]} \qquad (12)$$

It is useful to introduce a term

$$E^*_{\nu_{12}} = \frac{g_2\ c\ A_{21}}{g_1\ Y_{21}\ B_{12}} \qquad (13)$$

Using this expression and its predecessor and remembering $g_1B_{12} = g_2 B_{21}$,

$$\frac{n_2}{n_1} = \frac{g_2}{g_1} \left[\frac{E_{\nu_{12}}}{E_{\nu_{12}} + E^*_{\nu_{12}}}\right] \tag{14}$$

and

$$\frac{n_3}{n_1} = \frac{g_2}{g_1} \left[\frac{E_{\nu_{12}}}{E_{\nu_{12}} + E^*_{\nu_{12}}}\right] \left[\frac{k_{23}}{A_{31} + k_{31} + k_{32}}\right] \tag{15}$$

Rewriting Equation 2 for the case of ν_{12} absorption and emission yields

$$B_{F_{\substack{2\to1\\1\to2}}} = \left(\frac{r}{16}\right) Y_{21}\, h\, \nu_{12}\, E_{\nu_{12}}\, B_{12}\, n_1 \left[1 - \frac{g_1}{g_2}\frac{n_2}{n_1}\right] \tag{16}$$

Recalling that $n_1 + n_2 + n_3 = n_T$ and solving for n_1 in terms of n_T gives

$$n_1 = n_T \left[\frac{1}{1 + \frac{g_2}{g_1}\left(\frac{E_{\nu12}}{E_{\nu_{12}} + E^*_{\nu_{12}}}\right)\left(1 + \frac{k_{23}}{A_{31} + k_{31} + k_{32}}\right)}\right] \tag{17}$$

Substituting for n_1 and n_2/n_1 into Equation 16 gives

$$B_{F_{\substack{2\rightarrow 1\\1\rightarrow 2}}} = \left(\frac{r}{16}\right) A_{21}\, h\, \nu_{12}\, n_T \left[\frac{1}{1 + \frac{k_{23}}{A_{31} + k_{31} + k_{32}} + \frac{g_1}{g_2}\left(1 + \frac{E^*_{\nu_{12}}}{E_{\nu_{12}}}\right)}\right] \qquad (18)$$

The above expression describes completely the fluorescence radiance $B_{F_{\substack{2\rightarrow 1\\1\rightarrow 2}}}$ as a function of source irradiance $E_{\nu_{12}}$ in terms of fundamental constants, geometric factors and measurable experimental parameters. (The term $k_{23}/(A_{31} + k_{31} + k_{32})$ at first appears to contradict this statement; however, it is shown to be equal to n_3/n_2 in Equation 7 and may be determined by measuring the ratio of fluorescence from level 3 to the fluorescence from level 2 when the laser is tuned to ν_{12}.)

Figure 2 shows a log-log plot of Equation 18 on an arbitrary scale in order to demonstrate its shape and the various regions of interest. When $E_{\nu_{12}}$ is much less than $E^*_{\nu_{12}}$ (region I), the fluorescence radiance is directly proportional to the source irradiance, the log-log slope constant and equal to unity. In this region the excited state population is very small compared to that of the ground state. As $E_{\nu_{12}}$ approaches $E^*_{\nu_{12}}$ (region II), the fluorescence radiance no longer increases as fast as the source irradiance. The curve begins to bend over. The log-log slope is less than unity and decreases gradually. In this region, the excited

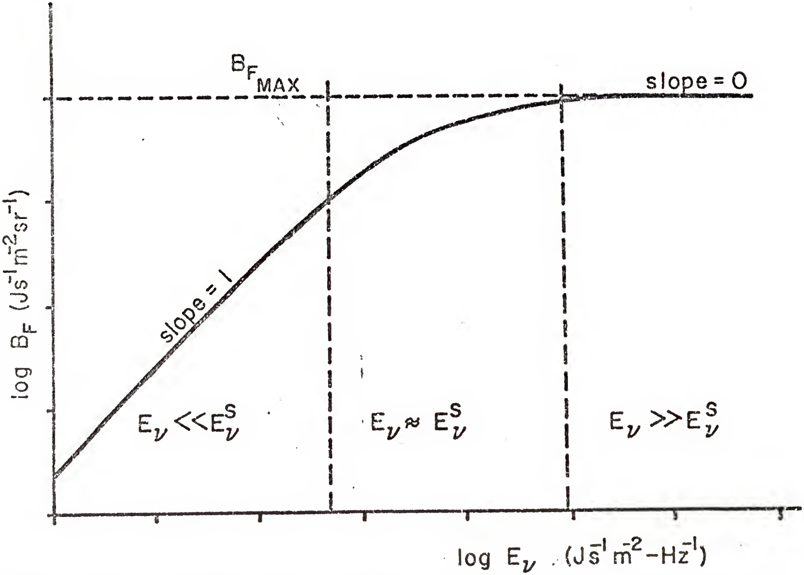

Figure 2. Typical saturation curve: log B_F vs. log E_ν. The three different regions are shown.

state concentration is smaller than, but comparable to that of the ground state, which is reflected by a decrease in the absorption coefficient k_ν. An increase in source irradiance results in a smaller increase in fluorescence than would result if the absorption coefficient were not decreasing. As $E_{\nu_{12}}$ reaches and exceeds $E^*_{\nu_{12}}$ (region III), the fluorescence radiance attains a maximum, the log-log slope equaling zero. In this region, the excited state concentration equals or approximates that of the ground state. (The statistical weights of the levels in the system determine the population ratios at saturation.) The important consequence is that the absorption coefficient has gone to zero. An increase in source irradiance results in no absorption and, therefore, no increase in fluorescence signal. It is helpful to rewrite Equation 18 for the two extreme cases of very low and very high source irradiances

$$B_{F_{\substack{2\to1\\1\to2}}(lo)} = (\frac{r}{16})\, A_{21}\, h\, \nu_{12}\, n_T\, [\frac{g_2}{g_1} \frac{E_{\nu_{12}}}{E^*_{\nu_{12}}}] \tag{18a}$$

$$B_{F_{\substack{2\to1\\1\to2}}(hi)} = (\frac{r}{16})\, A_{21}\, h\, \nu_{12}\, n_T\, [\frac{1}{1 + \frac{g_1}{g_2} + \frac{k_{23}}{A_{31} + k_{31} + k_{32}}}] \tag{18b}$$

Equation 18a shows the usual source intensity and quantum efficiency ($Y_{21} \propto 1/E^*_{\nu_{12}}$) dependence. In addition, the fluorescence signal is proportional to n_T, the relationship that allows quantitative analysis. Equation 18b shows that the maximum fluorescence radiance is still proportional to n_T but now the source irradiance and quantum efficiency dependence have vanished. This is the basic equation of saturation spectroscopy since it implies that absolute number densities can be obtained from a radiance measurement and knowledge of certain simple quantities (transition probabilities, photon energy, beam depth, etc.). Moreover, these absolute number densities are local, not line-of-sight, values due to the right angle observation of fluorescence.

Up to this point $E_{\nu_{12}}$ has been assumed to be a constant across the profile of the beam. Unfortunately, this is rarely the case, the intensity variations being a function of the laser cavity configuration, the tuning element, and optical aberrations. In some cases, the laser output intensity distribution follows a Gaussian profile (3). The fluorescence radiance in this case does not follow Equation 18. In order to arrive at an expression reflecting the spatial beam intensity variation, it is necessary to specify an illumination and collection geometry; this treatment follows Daily (16). As illustrated in Figure 3, this geometry will correspond to a vertical entrance slit cutting out a cylindrically shaped portion of the beam. The slit height, h, is much larger than the beam diameter, 2ω. For a Gaussian beam, the radial intensity distribution is

$$E_{\nu(r)} = E_{\nu}^{\circ} \exp\left(-\frac{r^2}{\omega^2}\right) \qquad (19)$$

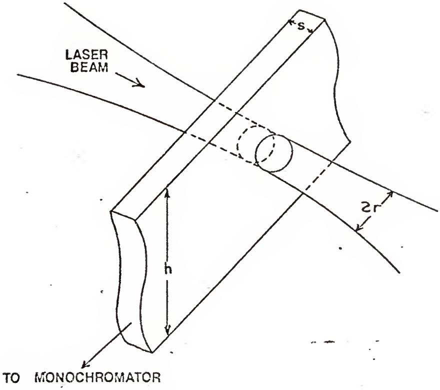

Figure 3. Beam geometry.

where

E°_ν = centerline beam irradiance, J s^{-1} m^{-2} Hz^{-1}; and

ω = (1/e) beam radius, m.

It is easiest to see the effect of a nonuniform source profile on B_F after writing Equation 18 in terms of n_2. Given that

$$n_2 = n_T \left(\frac{1}{1 + \frac{k_{23}}{A_{31} + k_{31} + k_{32}} + \frac{g_1}{g_2} \left(1 + \frac{E^*_{\nu_{12(r)}}}{E_{\nu_{12(r)}}}\right)} \right) \quad (20)$$

an equivalent expression is

$$n_2 = n_T \quad \frac{E_{\nu_{12(r)}}}{\frac{g_1}{g_2} E^*_{\nu_{12}} \quad \beta + E_{\nu_{12(r)}}} \quad (20a)$$

where

$$\beta = \frac{1}{1 + \frac{g_1}{g_2} + \frac{k_{23}}{A_{31} + k_{31} + k_{32}}}$$

Substituting Equation 20 into Equation 18 gives

$$B_{F_{\substack{2\rightarrow 1\\1\rightarrow 2}}} = \left(\frac{r}{16}\right) A_{21}\, h\, \nu_{12}\, n_2 \quad (21)$$

This is the usual emission equation where the signal is dependent only on the transition probability and the population of the excited state. In a more general form (which includes the polarization factor),

$$I_F = \frac{h\,\nu_{12}\,A_{21}}{8\pi} \int n_2\, dV \tag{22}$$

where

I_F = radiant intensity, J s^{-1} sr^{-1} ($I_F = B_F A$);

A = cross section of emission in direction of observation, m^2;

dV = observation volume, m^3.

In polar coordinates

$$I_F = \frac{h\,\nu_{12}\,A_{21}\,s}{8\pi} \int_0^\infty n_2\, 2\pi r\, dr \tag{23}$$

where s = width of emission observed, m (slitwidth). For a uniform circular beam n_2 does not vary with r (because $E_{\nu_{12}}$ is not a function of r) and may be taken out of the integral. Upon performing the integration

$$I_F = \frac{h\,\nu_{12}\,A_{21}\,n_2\,s\,r^2}{8} \tag{24}$$

which (using 2sr as the cross section of emission) reduces to Equation 21. However, if the beam profile is not uniform, then n_2 varies with r through the function $E_{\nu(r)}$ (see Equation 20). Equation 23 becomes

$$I_{F_{\substack{2\to1\\1\to2}}} = \frac{h\,\nu_{12}\,A_{21}\,s}{8\pi} \int_0^\infty n_T\, \beta\, \frac{E_{\nu_{12(r)}}}{\frac{g_1}{g_2}\, E^*_{\nu_{12}}\, \beta + E_{\nu_{12(r)}}}\, 2\pi r\, dr \tag{25}$$

which simplifies to

$$I_F = \frac{h\,\nu_{12}\,A_{21}\,n_T\,s\,\beta}{4} \int_0^\infty \frac{\exp\left(-\frac{r^2}{\omega^2}\right) r\,dr}{\frac{g_1}{g_2}\frac{E^*_{\nu_{12}}}{E^\circ_{\nu_{12}}}\beta + \exp\left(-\frac{r^2}{\omega^2}\right)} \qquad (26)$$

Upon performing the integration

$$I_F = \frac{h\,\nu_{12}\,A_{21}\,n_T}{8}\,\beta\,\omega^2\,s\,\log\left[1 + \frac{E^\circ_{\nu_{12}}}{E^*_{\nu_{12}}}\,\frac{g_2}{g_1}\,\frac{1}{\beta}\right] \qquad (27)$$

Solving for $B_{F_{\substack{2\to1\\1\to2}}}$ (using $2s\omega$ as the cross section of emission yields

$$B_{F_{\substack{2\to1\\1\to2}}} = \left(\frac{\omega}{16}\right) h\,\nu_{12}\,A_{21}\,n_T\,\beta\,\log\left[1 + \frac{E^\circ_{\nu_{12}}}{E^*_{\nu_{12}}}\,\frac{g_2}{g_1}\,\frac{1}{\beta}\right] \qquad (28)$$

Plots of Equations 18 and 28 are compared in Figure 4. In the saturation region ($E_{\nu_{12}} >> E^*_{\nu_{12}}$), the curve does not flatten out when the beam profile is nonuniform. If the source irradiance is increased in this region, no additional fluorescence will originate from the central portion of the beam. However, at some distance away from the center, the transition is no longer saturated, and the fluorescence radiance will follow the source irradiance. There is no plateau in the saturation region when the beam profile is nonuniform; the exact shape of the B_F vs. E_ν curve here is determined by the beam's intensity function. For a Gaussian profile, the curve continues upwards as the log of $E_{\nu_{12}}$. In the low source

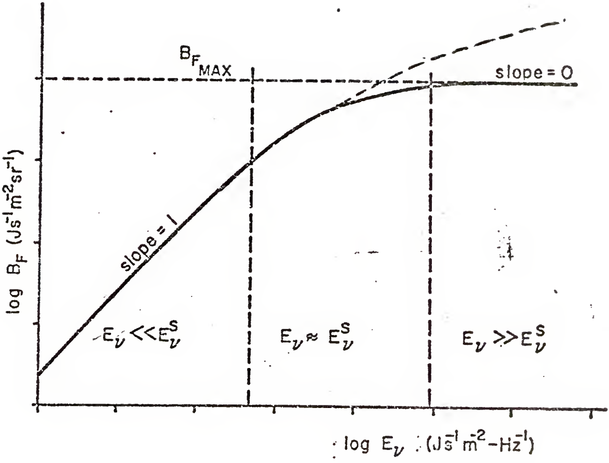

Figure 4. Log B_F vs. log E_ν. Solid curve: uniform beam; dashed curve: Gaussian beam.

intensity region ($E_{\nu_{12}} << E^*_{\nu_{12}}$), Equation 28 reduces to Equation 18a as it must because the beam's intensity variation has no effect on the fluorescence signal until saturation is approached.

Experiment

Before a detailed description of the experimental apparatus and prodecure is undertaken, an examination of the assumptions on which the theory is based will be made.

(i) Atomic sodium provides, as mentioned before, a good approximation to a three-level system. The $3^2P_{\frac{1}{2}}$ and $3^2P_{3/2}$ levels, the first excited states, are located 2.1 eV above the ground state. The next available level above this doublet is the 4^2P state lying 3.7 eV above the ground state. At a flame temperature of 2000 K, >99.999% of the total population is in the first three levels.

(ii) Self-absorption is usually considered negligible when $k_\nu b \leq 0.05$, where k_ν = absorption coefficient and b = absorption path length. All experiments were performed under these conditions.

(iii) Laser induced medium heating is found to be insignificant in "clean" combustors, i.e., no soot particulates (17).

(iv) The temperature and concentration homogeneity of the flame was safeguarded by the use of an argon sheathed, flame shielded inner flame. The inner and outer flames were of the same composition, analyte being introduced into the inner flame only. This arrangement precluded edge effects and entrainment of room air.

(v) The laser used in this work was an Ar^+-pumped dye laser. The bandwidth of the dye laser was specified to be 40 GHz; a measurement of the bandwidth with a 1 m monochromator, 10 μm slits, 0.8 nm/mm dispersion, gave 45 GHz, in good agreement with the manufacturer's value. This width describes the 1/e width of the envelope that contains the narrow, individual longitudinal modes which are spaced at an interval of $\Delta\nu = c/2L$, 300 MHz, and have a width of 7 MHz. An illustration of this envelope is shown in Figure 5. Over a typical atomic absorption linewidth in the flame of ≈10 GHz (18), there are about 30 individual spectral components. The atom line profile is superimposed on the laser output in Figure 5. The assumption is made, then, that the laser approaches a continuum source.

(vi) The response times of the absorption, emission, and collisional processes involved in this work are on the order of nanoseconds. The chopping frequency of the laser was 250 Hz, the source being on for 2 milliseconds. The response times were therefore much smaller than the laser on-time, allowing steady state conditions to be reached easily.

A block diagram of the basic experimental system is shown in Figure 6. A cw 5 W Ar^+ laser is used to pump a tunable dye laser. The output of the dye head is chopped

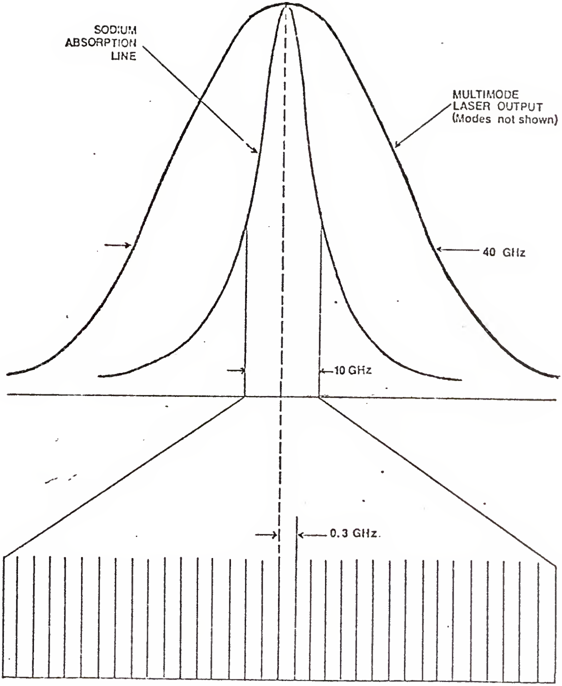

Figure 5. Comparison of multi-mode laser linewidth, individual mode spacing, and atomic absorption linewidth.

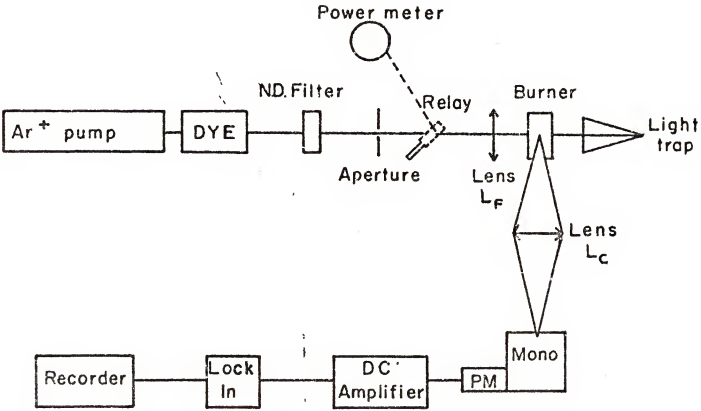

Figure 6. Block diagram of experimental system

at the reference frequency, allowed to diverge slightly before passage through neutral density filters, focused by a lens to a point in the flame. The burner consisted of a commercially available Perkin-Elmer premix aspiration chamber with pneumatic nebulizer which was fitted with a laboratory constructed brass head. The inner and outer burners were rectangular as was the sheath. The collection lens L_c projects a 1:1 image of the laser pencil on the entrance slit of the monochromator placed at right angles to the laser beam. The photocurrent at the exit of the PM tube was amplified and sent to a lock-in which subtracted out the dc background and produced a voltage proportional to the signal at the reference frequency, i.e., proportional to the signal produced by the laser. This was displayed on a strip chart recorder. Positioned immediately before the laser focusing lens L_F was a mirror on a relay which deflected the beam into a power measuring device. Table I gives the details of all experimental components.

An experimental verification of Equations 18 and 28 required: (i) measurement of source power; (ii) measurement of the laser beam size and profile at the point of excitation; (iii) measurement or knowledge of the quantum efficiency Y (in order to determine E*); (iv) measurement of n_T, the total atom concentration; and (v) measurement of an absolute radiance which requires calibration of the collection and detection systems with a standard source.

Table I
Experimental Components and Manufacturers

Item	Model No.	Source
Argon Ion Laser	552	Control Laser Corp., Orlando, FL
Cw Dye Laser	590	Coherent Radiation, Palo Alto, CA
Tungsten Strip Lamps	EP UV 1068 EP UV 1104	Eppley Laboratory, Inc., Newport, RI
Photomultiplier Tube	R818	Hamamatsu Corp., Middlesex, NJ
Photomultiplier Housing	180	Princeton Applied Research, Princeton, NJ
H. V. Power Supply	244	Keithley Instruments, Cleveland, OH
Monochromator	1870	Spex Industries, Metuchen, NJ
Strip Chart Recorder	Servoriter II	Texas Instruments Corp., Houston, TX
Current-to-Voltage Converter	427	Keithley Instruments, Cleveland, OH
Lock-in Amplifier	840	Keithley Instruments, Cleveland, OH
Laser Power Meter	210	Coherent Radiation, Palo Alto, CA
Strip Lamp Power Supply	-	Laboratory Constructed, 0 - 50 A, 12 V DC, University of Florida
Flow Meters	E29-R-150mm4 E29-4-150mm3	Air Products Corp., Allentown, PA
Burner Nebulizer	303-0110	Perkin-Elmer, Norwalk,CT
Front Surface Mirrors	02-MPQ-001-023	Melles Griot, Irvine, CA

(i) The laser power was monitored by means of a calibrated PIN photodiode onto which the beam was deflected by the relay mirror. The diode was linear in response over five orders of magnitude of illumination. Power losses due to reflection and absorption at the lens L_F were less than 10%.

(ii) The beam size was determined by removing the burner and putting a microscope in its place. The beam was viewed while a good scattering medium (smoke) was introduced. Using a calibrated eyepiece, it was observed and measured. The beam was examined with and without lens L_F in place (beam focused and unfocused). Under the microscope with smoke introduced, the beam was a bright stripe with sharp edges; the width of the stripe appeared to be unambiguous. The beam profile was constructed by scanning a small pinhole (250 μm) across the beam and recording the intensity falling on a photodiode behind the pinhole. Profiles were made of the unfocused beam and of the focused beam after it had diverged to an acceptable degree. (A profile of the beam at the focal point was not possible because of the limited pinhole size.) The assumption was made that the intensity distribution at the focal point would be identical to that of the diverged, focused beam. These results and a Gaussian profile are shown in Figure 7. The profiles did not extend very far into the wings because of background light from the laser itself. Scatter off room dust was sufficiently high to preclude the possibility of

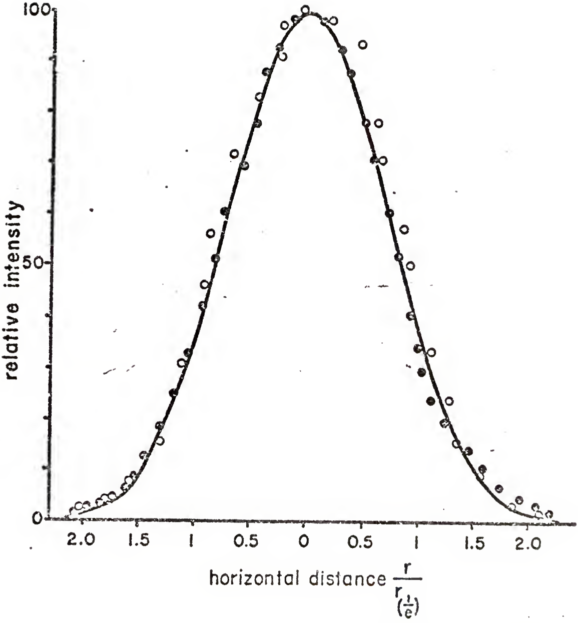

Figure 7. Normalized horizontal profiles of laser beam.

monitoring the beam distribution well into the wings. The effect of neutral density filters on the beam profile was negligible as long as the surfaces were clean and the beam large (> 1 mm) when traversing the filter. When the beam was unfocused, the 1/e diameter corresponded to 2/3 of the width of the stripe measured under the microscope. The same relationship was assumed to hold for the focused beam.

(iii) The measurement of a quantum efficiency Y is a tedious and involved process. Fortunately, the quenching rate constants k_{21} and k_{31} for the $3^2P_{\frac{1}{2},3/2} - 3^2S_{\frac{1}{2}}$ transitions of sodium have been determined by several groups of workers (19-23). Flames identical to those studied by Hooymayers and Alkemade (22) were set up in order to obviate a direct measurement of Y_{21}. Flame gases were all standard commercial grades. After two stage regulation at the cylinders, the gases passed through calibrated rotameter flow meters fitted with needle valves. Additional premix chambers were placed in series after the valves to insure homogeneity at the point of combustion. Characteristic experimental parameters for the two flames used are given in Table II. The rate constants k_{21} and k_{31} were taken from reference 22, A_{21} and A_{31} from reference 24, and the ratio $k_{23}/(A_{31} + k_{31} + k_{32})$ determined experimentally as previously described in the text following Equation 18. (At this point, it should be noted that since $k_{32} = (g_2/g_3) \exp (E_{32}/kT)$ and $E_{32} << kT$ at 2000 K, $k_{32} = (g_2/g_3)k_{23} = \frac{1}{2}k_{23}$. Substitution of these values into Equation 12 allows evaluation of Y_{21} and $E^*_{\nu_{12}}$.

Table II
Flame Parameters

	Ratio of flow rates I = inner flame, O = outer flame									
	H_2		O_2		Inert		k_{21}^*	meas.	calc.	meas.
	I	O	I	O	I	O	(s^{-1})	n_3/n_2	$Y^†$	n_T (m^{-3})
#3* Ar diluted	2	4	1	2	7	14	0.35×10^8	1.9	0.21	1.6×10^{17}
#6* N_2 diluted	2	4	1	2	7	14	11×10^8	1.4	0.017	9.6×10^{16}

[*] From reference 22

[†] Using relationship in Equation 12

(iv) A value of n_T may be obtained by a measurement of the total absorption of the flame against a background continuum source at the wavelength of the transition of interest. The continuum source was a 300 W Eimac lamp which was placed on a line of sight with the flame, collection optics, and monochromator. The radiation from the lamp was chopped and focused to the flame center. The theory and procedure has been outlined by Zeegers et al. (25). The total atomic concentration is given by

$$n_T = \frac{m\ c^2\ Z\ \Delta\lambda_m\ \alpha}{\pi\ e^2\ \lambda_o^2\ f\ b\ g_o} \tag{29}$$

where

m = electron mass, kg;

e = electron charge, $m^{3/2}\ kg^{\frac{1}{2}}\ s^{-1}$;

λ_o = peak wavelength of absorption, m;

f = oscillator strength, dimensionless;

b = absorption pathlength, m;

Z = electronic partition function for the absorber, dimensionless;

g_o = statistical weight of electronic ground state, dimensionless;

$\Delta\lambda_m$ = spectral bandpass of monochromator, m; and

α = measured fraction of incident intensity absorbed, dimensionless.

Values of these parameters and n_T are shown in Table III.

Table III
Values Used in Determining n_T for Two Flames
by the Method of Total Absorption

$m = 9.11 \times 10^{-31}$ kg

$e = 4.80 \times 10^{-15}$ $m^{3/2}$ $kg^{\frac{1}{2}}$ s^{-1}

$\lambda_o = 589.6 \times 10^{-9}$ m

$f = 0.327$

$b = 0.012$ m

$Z = 2$

$g_o = 2$

$\Delta\lambda_m = 5.1 \times 10^{-11}$ m

$c = 3.0 \times 10^{8}$ m s^{-1}

$n_T = 4.2 \times 10^{18}\ \alpha$

$\alpha_{N_2} = 0.023$

$n_{T_{N_2}} = 9.6 \times 10^{16}$ m^{-3}

$\alpha_{Ar} = 0.038$

$n_{T_{Ar}} = 1.6 \times 10^{17}$ m^{-3}

(v) The measurement of an absolute radiance requires use of a standard source, the usual choice in the visible being a calibrated W strip lamp. The burner was removed and replaced by the lamp so that the center of the tungsten filament coincided with the focal point of the laser beam. A calibration factor was then obtained by measuring the photocurrent corresponding to the known spectral radiance of the standard lamp and accounting for the difference in area viewed of the filament and laser beam as follows

$$C = \frac{i_D}{(B^\circ_{lamp})(\Delta\lambda_m)} \frac{A_L}{hs} \tag{30}$$

where

C = calibration factor, A J^{-1} m^2 s sr;

i_D = detector photo anodic current, A;

B°_{lamp} = absolute spectral radiance of the lamp at λ_o, J s^{-1} m^{-2} sr^{-1};

hs = area of filament observed, m^2 (slit height x slit width); and

A_L = area of laser beam observed, m^2.

The calibration was performed with two different lamps and the results agreed to within 5%.

Experimental curves of log B_F vs. log E_ν were constructed for the two flames. The source irradiance was varied over six orders of magnitude by measuring fluorescence with and without the focusing lens L_F. In each case neutral density filters were used to attenuate the beam. In order to show focused and unfocused results on the same graph log B_F/r is plotted vs. log E_ν. Results for the two flames are shown in Figures 8 and 9 along with the theoretical curves of Equations 18 and 28. The theoretical curves were generated by using the measured values of r, ω, n_T, β and the rate constants k_{21} and k_{31} determined in reference 21.

The overall agreement between them is rather good; however, the shapes of the experimental curves deviate from both theoretical expressions at high source irradiances, the Gaussian profile treatment extending agreement slightly further than that of the uniform beam. This emphasizes the point that the profile of the exciting beam's wings must be known in order to correctly predict the dependence of B_F on E_ν at high source irradiances. Ignorance of the laser beam's profile when performing saturation measurements will result in errors in the determination of n_T. The concept of $B_{F\max}$ (the plateau fluorescence radiance) is lost and a value of n_T may be determined only by an arbitrary criterion of deviation from linearity of log B_F vs. log E_ν.

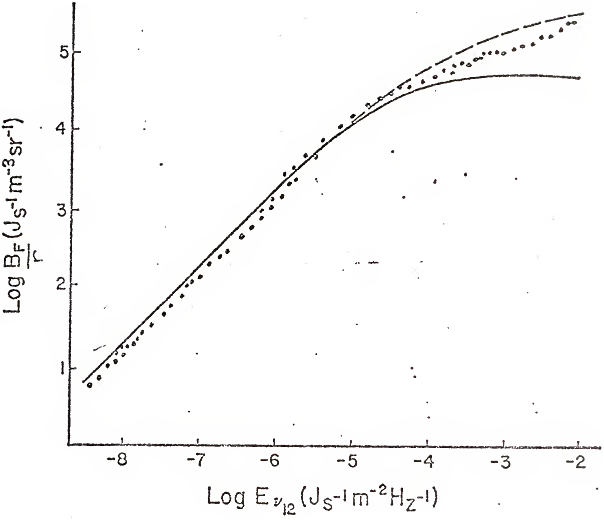

Figure 8. Comparison of experimental and theoretical results for flame # 3.
Solid curve: Equation 18 using parameters of Table II (theory)
Dashed curve: Equation 28 using parameters of Table II (theory)
● : Experimental data.

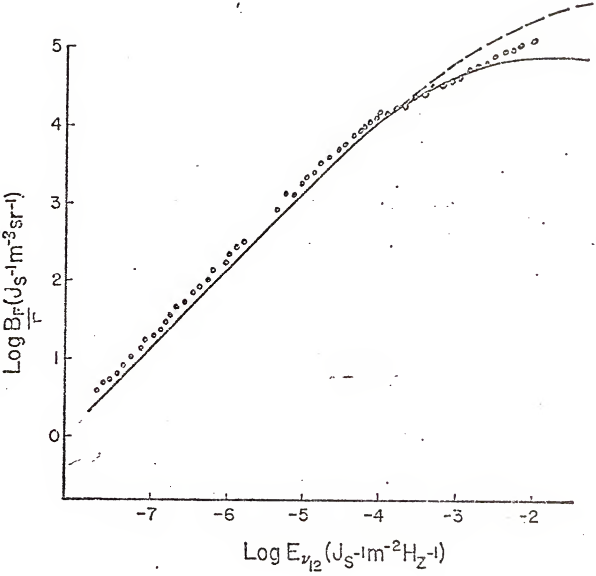

Figure 9. Comparison of experimental and theoretical results for flame # 6.

Solid curve: Equation 18 using parameters of Table II (theory)

Dashed curve: Equation 28 using parameters of Table II (theory)

● : Experimental data.

CHAPTER III
MOLECULAR FLUORESCENCE IN FLAMES

Molecular emission, absorption and fluorescence spectra contain information about the molecule's geometric and energetic configuration. Molecular fluorescence offers the advantage of populating some specific excited state by absorption and observing the different emission pathways back to the ground state. In a flame the molecules in the excited state undergo collisions with flame gas molecules, exchanging energy. At atmospheric pressure, collisions may significantly decrease the excited state lifetime. By using a laser with narrow spectral bandwidth as the excitation source, it is possible to populate a small range of rotational levels within a given vibrational state within a given electronic state: $\Delta E_L = h\ \Delta\nu_L \simeq 1\ cm^{-1}$ at 600 nm. The fine structure of the resulting fluorescence spectra may reveal the extent of vibrational and collisional mixing of rotational levels. For these reasons, molecular fluorescence in flames is a phenomenon of interest.

Until recently, the study of molecular fluorescence of flame species has been limited by the difficulty of its observation. In general, molecular fluorescence spectra are quite weak and may require signal averaging to enhance the S/N (26,27). By using a cw laser, it is possible to excite molecular fluorescence that is observable in real time with conventional synchronous detection. The main constraint to its use as a source is, as mentioned previously, the tunability range of the laser (540 - 700 nm, undoubled with a 5 W Ar^+ pump). There are not many molecules which exist in flames and have sufficiently intense absorption bands in this spectral region. C_2 is a pleasant exception, and certain metal oxides also fulfill these requirements if a relatively cool flame is provided.

Experiment

The experimental system shown in Figure 10 differs from that of Figure 6 only in the collection geometry. The dove prism between the flame and entrance slit of the monochromator rotates the horizontal stripe of laser excited fluorescence 90° so that the entire slit height (1 cm) was filled, resulting in an increased S/N which facilitated the recording of spectra. Either the monochromator or the dye laser could be scanned. A Perkin-Elmer nebulizer was used with a laboratory constructed 1 cm optical path length capillary burner head. Two different flames were utilized: (i) for the metal oxides studies, a premixed Ar - O_2 - H_2 flame; and (ii) for the C_2 studies, a premixed Ar - O_2 - C_2H_2 flame. Experimental conditions are summarized in Table IV. The height of observation was optimized for each species. In the C_2 studies, it was necessary to work at the top of the blue-green cones of

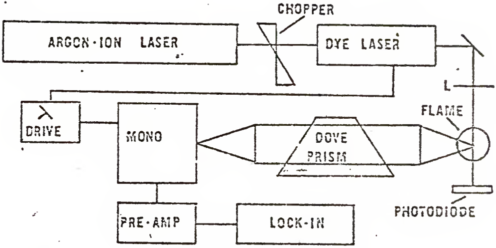

Figure 10. Block diagram of experimental system. L, focusing lens.

Table IV
Characteristics of the Experimental System

I. Source Characteristics: Cw tunable dye laser pumped by a cw 5 W Ar^+ laser

   A. Tunability range: 540 - 630 nm

   B. Power: 200 - 900 mW

   C. Bandwidth: ≈0.05 nm

II. Flame Characteristics

   A. Premixed Ar - O_2 - H_2: 6.1 ℓ min^{-1}, 1.6 ℓ min^{-1}, and 3.2 ℓ min^{-1}, respectively

   B. Premixed Ar - O_2 - C_2H_2: 5.2 ℓ min^{-1}, 1.3 ℓ min^{-1}, and 1.2 ℓ min^{-1}, respectively

III. Detector Characteristics

   A. Reciprocal linear dispersion: 1.6 nm/mm

   B. Slit width: 20 - 400 μm

   C. PM tube: R818 Hamamatsu

the flame where the C_2 concentration was very large. All metal solutions were prepared from reagent grade chemicals and ranged in concentration from 5000 to 10 000 mg/l.

The molecular fluorescence spectra of five species were observed in this work. Two of these five, CaOH and SrOH, have been previously reported by Human and Zeegers using an Eimac xenon arc continuum source (28). Results for the alkaline earth monohydroxides will be discussed only briefly because little is presently known about the geometric and energetic configurations and because of the previous studies. The fluorescence spectra of two other species, CrO and MnO, were recorded for the first time and will be discussed in more detail. C_2 fluorescence has been observed by several workers (8,27,29). Jones and Mackie (29) used the 514.5 nm line of a cw Ar^+ laser, whereas the other two groups (8,27) used a pulsed dye laser. In this study, cw laser excited flame fluorescence spectra are contrasted with flame emission spectra.

SrOH

The emission spectrum is given in Figure 11 (30,31); the band at 606 nm exhibiting several fine features can be seen in more detail in Figure 12. The red bands (647 - 682 nm) are diffuse. When the excitation source was tuned to the maximum at 606 nm, fluorescence was detected at the resonance wavelength and over the entire emission system. As Human and Zeegers reported, there was no difference in the

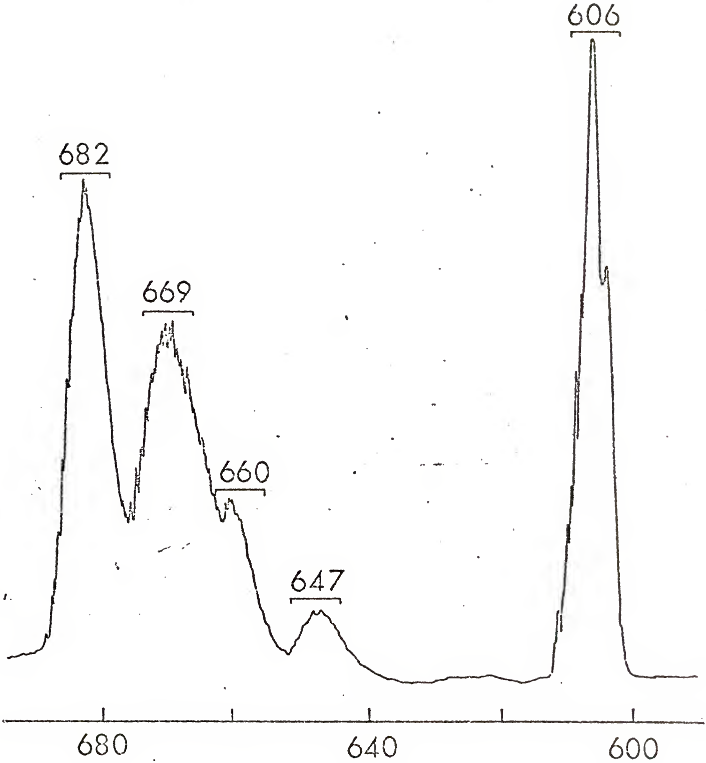

Figure 11. Flame emission spectrum of SrOH. The x-axis is wavelength, nm.

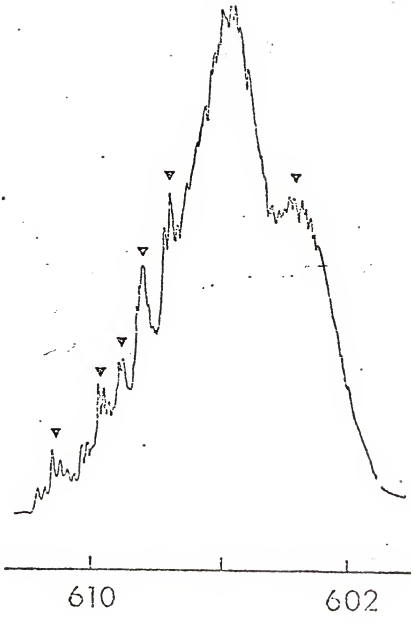

Figure 12. Flame emission spectrum of SrOH (606 nm band).
The x-axis is wavelength, nm.

shape of the emission and fluorescence bands and the relative intensity of the band maxima are equal in fluorescence and emission. To repeat, the shape and relative intensity of maxima which resulted from using a source with a 0.05 nm bandwidth were the same as those which resulted from using a continuum source.

The effect of variation in excitation wavelength on fluorescence intensity is shown in Figure 13. The monochromator was fixed at the band maximum near 682 nm, and the laser was scanned across the band at 606 nm. The structure of the 606 nm excitation band was reflected by changes in fluorescence intensity at 682 nm.

As shown in Figure 12, there are several discernible fine features in the band at 606 nm; side peaks occur at 604.0 nm, 607.6 nm, 608.4 nm, 609.0 nm, 609.6 nm, and 611.0 nm (30,31). These features are marked in the figure. When the laser was tuned to each of these side peaks and the monochromator scanned across the entire band, the fine features were altered. In Figure 14, six fluorescence spectra having different excitation wavelengths are shown. There was a change in the shape of the band peak and the appearance of two new side peaks near 605.2 nm when the laser was tuned to 604 nm (spectrum 5). With the laser at 607.7 nm, a new peak occurred at 604.6 nm (spectrum 3). With the laser at 608.5 nm, a new peak occurred at 606.9 nm (spectrum 2).

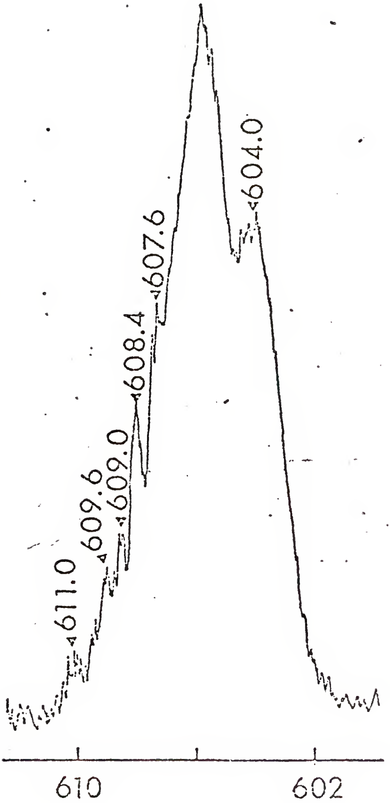

Figure 13. Fluorescence spectrum of SrOH. Monochromator fixed at 682 nm. The x axis is the excitation wavelength, nm

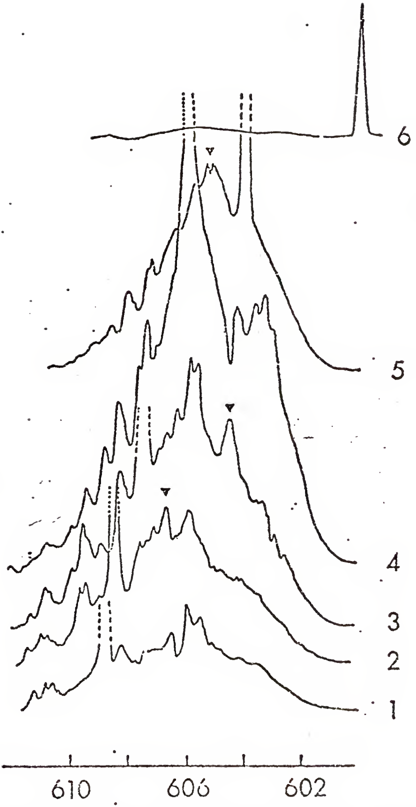

Figure 14. Flame fluorescence at 606 nm as a function of excitation wavelength. Excitation at: 1) 609.0 nm; 2) 608.5 nm; 3) 607.7 nm; 4) 606.0 nm; 5) 604.0 nm; 6) 600.0 nm.

CaOH

When solutions of calcium were aspirated into the flame, CaOH emission and fluorescence were observed. The emission bands have roughly the same shapes as those of SrOH but are shifted approximately 50 nm toward the blue and show less detail (30,31). The fluorescence characteristics of CaOH and SrOH closely resembled each other. In Figure 15, the emission and fluorescence spectra of CaOH are given.

CrO

A partial energy level diagram of CrO ($A^5\Pi$ - $X^5\Pi$) is shown in Figure 16 (32). The emission bands are degraded to the red. The laser was tuned to transitions at either 579 nm or 605 nm. With excitation at either of these two wavelengths, fluorescence transitions originating from the same upper level were observed; the fluorescence was in the form of bands. For example, with excitation at 605 nm, fluorescence was recorded at 605 nm, 639 nm, and 677 nm.

In Figure 17, the bands at 605 nm and 639 nm, which appear in emission as superimposable quintets (33), are shown. When the monochromator was set at the peak wavelengths of each of the five substates at 639 nm and the laser scanned across the five substates at 605 nm, fluorescence maxima occurred when the laser was pumping the same substate as the monochromator viewing, e.g., excitation at 605.2 nm (Σ = -1), fluorescence maximum at 639.2 nm (Σ = -1). In Figure 18, three representative spectra are shown. To determine

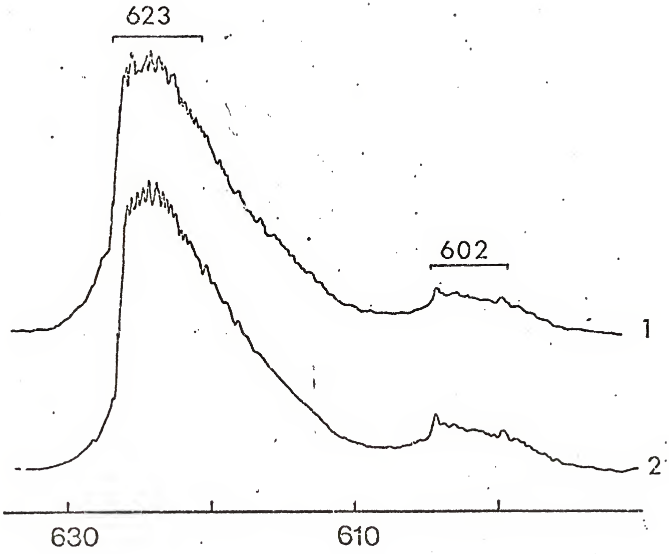

Figure 15. 1) CaOH flame emission
2) CaOH flame fluorescence with laser excitation at 554 nm.
The x axis is wavelength, nm.

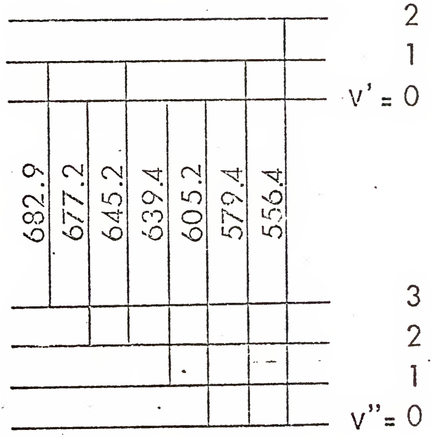

Figure 16. Partial energy level diagram for CrO ($A^5\Pi$ - $X^5\Pi$).

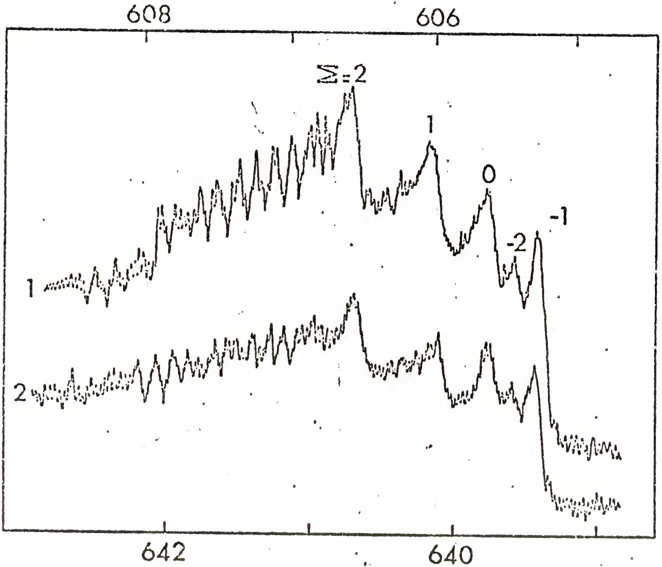

Figure 17. Flame emission spectra of CrO. Upper spectrum: (0 - 0) band. Lower spectrum: (0 - 1) band. The x axis is wavelength, nm.

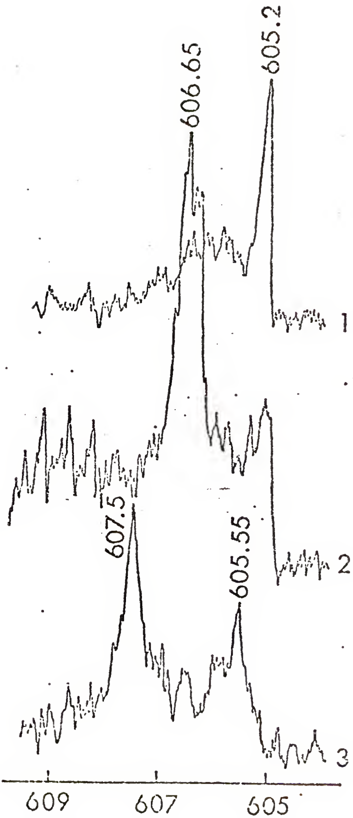

Figure 18. Flame fluorescence spectra of CrO. Monochromator at: 1) 639.2 nm; 2) 640.7 nm; 3) 641.5 nm. The x axis is the excitation wavelength, nm.

if this effect was confined only to band heads, the monochromator was set at two arbitrary wavelengths within the rotational structure of the tail of the 639 nm band; a fluorescence maximum was observed when the laser reached a wavelength in the tail of the 605 nm band as shown in Figure 18 (spectrum 3). In addition, a second smaller maximum occurred in both of these cases. The difference between the excitation energy and the main fluorescence peak energy was constant and had a value of approximately 870 cm^{-1}. In Figure 19, a graph of the fluorescence peak energy vs. excitation energy is given. The two secondary maxima are also plotted.

MnO

A partial energy diagram of MnO is shown in Figure 20. The two electronic states involved are assumed to be the ground and first excited state (32). The emission bands are degraded to the red. The laser was tuned to all transitions shown in Figure 20; however, several of these transitions involve sparsely populated lower states ($v'' > 3$) and yielded only weak fluorescence signals. Generally, for a given wavelength of excitation, fluorescence transitions originating from the same and adjacent ($v' \pm 1$) upper levels were observed where v' = upper vibrational level of absorption transition. When the laser was fixed at the peak of an emission band, nonresonance fluorescence peaks were observed at wavelengths near, but not coincident with,

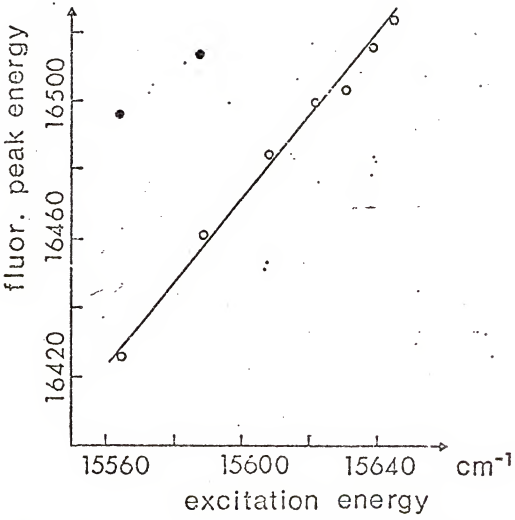

Figure 19. Energy of fluorescence maxima, cm^{-1}, vs. excitation energy, cm^{-1}.
o: primary maxima
●: secondary maxima.

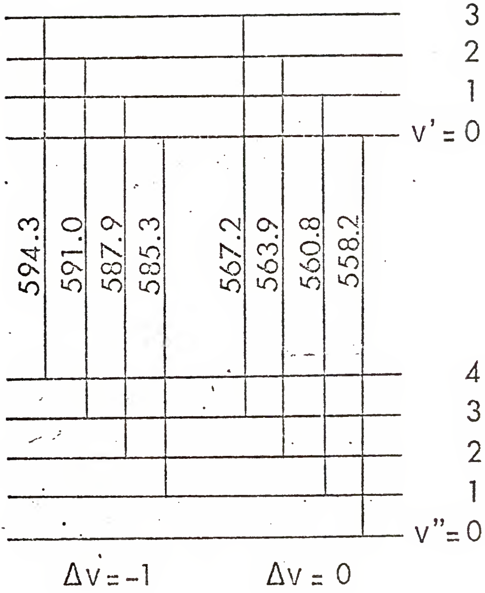

Figure 20. Partial energy level diagram for MnO.

emission band heads. These peaks contained no rotational fine structure and had half-widths determined by the spectral bandpass of the monochromator. This effect is clearly shown in Figure 21, where the emission spectrum is superimposed on the fluorescence spectrum.

When the laser was tuned to several wavelengths from 558 nm to 563 nm (through the (0 - 0) and (1 - 1) bands) and the monochromator scanned from 585 nm to 591 nm, fluorescence maxima occurred as in the case of CrO but with two peaks (from excitation of the (0 - 0) and (1 - 1) band). It was also possible to observe a weak third peak (from the excitation of the (2 - 2) band). In Figure 22, plots of wavelength of the two fluorescence maxima vs. excitation wavelength are given. Band head locations are denoted on each axis.

The MnO fluorescence spectra differed from CrO in that excitation at a band head of MnO led to fluorescence near another band head but not on the band head as shown in Figure 22. The reason for the discontinuities in the two MnO plots is not known.

C2

A partial energy level diagram for C_2 ($A^3\Pi_g$ - $X^3\Pi_u$) is shown in Figure 23. The bands are degraded to the blue and possess well separated rotational fine structure (34). When the dye laser was tuned to a given transition, fluorescence was observed from states having the same upper level or a lower adjacent (v' - 1) upper level. Fluorescence from an upper adjacent (v' + 1) level was weak. Unlike the cases

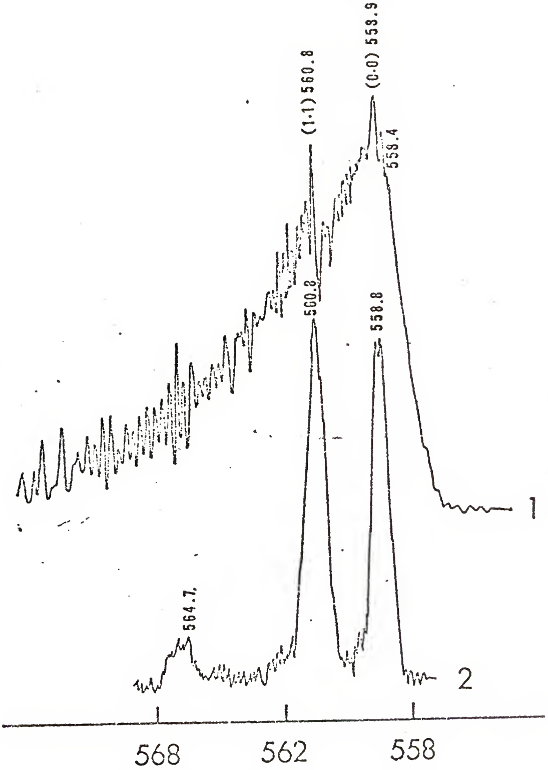

Figure 21. 1) MnO flame emission
2) MnO flame fluorescence with laser excitation at 587.9 nm.
The x axis is wavelength, nm.

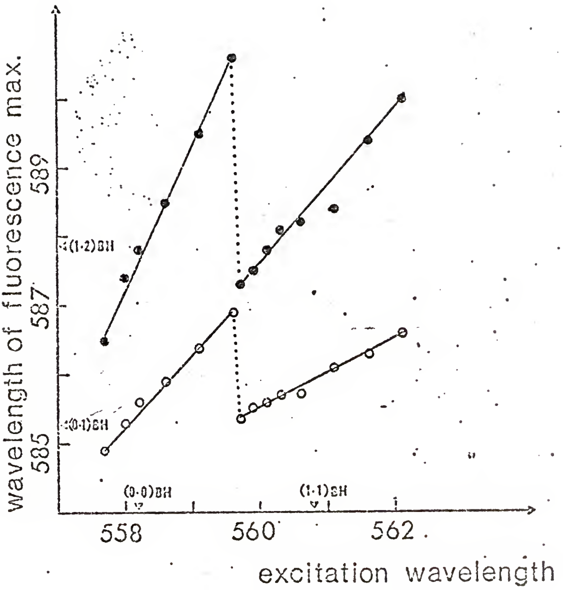

Figure 22. Wavelength of fluorescence maxima, nm, vs. excitation wavelength, nm, for MnO.
●: fluorescence peak located in (1 - 2) band.
o: fluorescence peak located in (0 - 1) band.

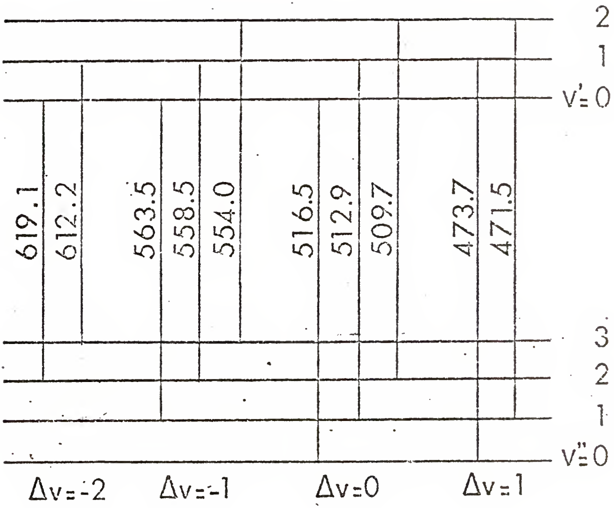

Figure 23. Partial energy level diagram for C_2 ($A^3\Pi_g$ - $X^3\Pi_u$)

of CrO and MnO, rotational fine structure was observed in fluorescence when the band head was excited. In Figure 24, the C_2 fluorescence and emission spectra at 516 nm are shown. The wavelengths of the band heads in emission and fluorescence coincide. A careful comparison of the fine structure of the 516 nm band reveals that the intensity of R-branch of the (0 - 0) band is enhanced compared to the P-branch.

BaO

Although BaO ($A^1\Sigma - X^1\Sigma$) appears to fulfill the requirements for yielding molecular fluorescence, it was not observed under our experimental conditions.

Conclusion

It is difficult to account for the differences in the flame fluorescence spectra obtained because of the paucity of information on the molecules investigated. Except for C_2, the rotational structure either is not known or is too diffuse to allow resolution with our experimental system. Also, any general principles of behavior would emerge only after the examination of many more molecules. The investigation of fluorescence of well characterized molecules (e.g., N_2, OH, CH) would be interesting.

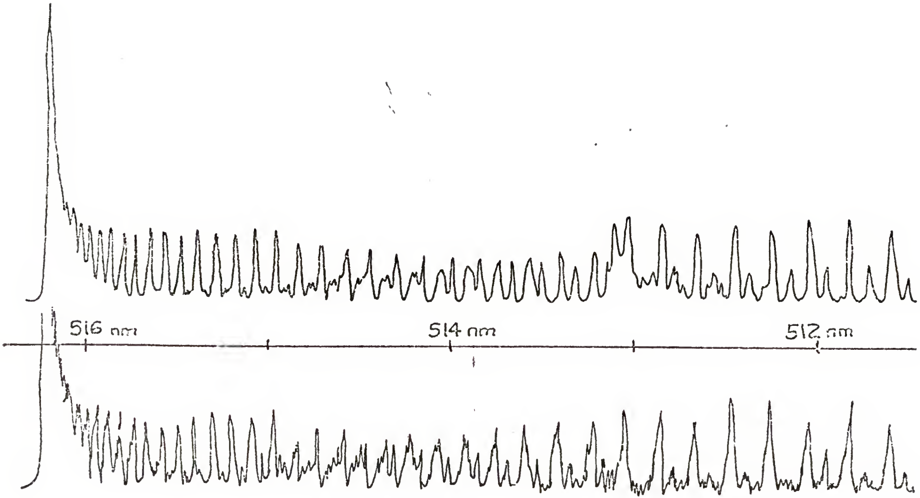

Figure 24. Upper: C_2 flame emission. Lower: C_2 flame fluorescence with laser excitation at 563 nm. The x axis is wavelength, nm.

APPENDIX

The limit of detection (LOD) is a figure of merit which provides a basis of comparison of different methods of analysis. It is dependent on the signal arising from a standard of known analyte concentration and the noise associated with the blank (standard minus analyte). As the analyte concentration in the standard is decreased, the analyte signal also decreases and ultimately becomes equal to, and indistinguishable from, the noise on the blank. The LOD is related to the value of the analyte concentration at which this occurs.

It is impossible, therefore, to evaluate an excitation source for analytical fluorescence spectrometry without consideration of the noise on the blank which may or may not be source related. Of course, the total noise on the blank is a combination of contributions from several different processes. It would be helpful to know the fraction of the total blank noise which is laser modulated in order to decide if the source fluctuations pose a limitation to improvement of the LOD.

A short study was made of the noises present in the experimental system of Figure 6 using the components listed in Table I. The output voltage of the lock-in amplifier was integrated for ten seconds and sixteen integrations were performed for each configuration of the experimental system. The standard deviation of the sixteen integrations was taken to be proportional to the total rms noise present. The individual contributions to the total noise were assumed to be independent and to add quadratically. The relative contribution of each process, σ_i, and the total noise, σ_T, is shown in Table V. The measurements were made with the laser at 553 nm.

According to this data, laser modulated Rayleigh and/or Mie scatter make the largest single contribution to the noise on the blank. The shot noise component of this scatter noise is very small. However, even if all laser associated noises were eliminated, the noise on the blank would decrease by only about a factor of 10. Flame background noise contribution becomes significant at that point. It is questionable whether or not a hotter, higher background flame (such as N_2O - C_2H_2) would provide better LOD's. Analyte signal levels would rise because of increased atomization efficiency, but the flame background noise would also grow in most spectral regions; for elements forming refractory oxides, like Mo, Ta, W, Si, Al, etc., the gain in atomization efficiency should greatly outweigh the increase in flame background noise. The shot noise on the dark current serves as a lower limit of the blank noise. It is interesting to note that further improvement of LOD's in the system beyond this noise limitation can be made only by increasing analyte

Table V
Noise Evaluation

	σ_T	σ_i
shorted input to amplifier	0.04	0.04
PM dark current	0.16	0.15
50/50 slits, room lights dimmed	0.28	0.23
flame lit	0.45	0.35
flame + laser	0.90	0.78
flame + laser + water blank	2.0	1.8
flame + laser + 10 ppm La blank	4.8	2.7

signals; the phenomenon of saturation, discussed in the second chapter, determines the maximum analyte signal obtainable.

REFERENCES

1. T. W. Hänsch, "Applications of Dye Lasers," chapter in Dye Lasers, F. P. Schafer, ed., Springer Verlag, New York (1973).
2. R. M. Measures, J. Appl. Phys., 39, 5232 (1968).
3. A. B. Rodrigo and R. M. Measures, IEEE J. Quant. Elect., QE-9, 973 (1973).
4. J. W. Daily, Appl. Opt., 15, 955 (1976).
5. E. H. Piepmeier, Spectrochim. Acta, 27B, 431 (1972).
6. N. Omenetto, P. Benetti, L. P. Hart, J. D. Winefordner, and C. Th. J. Alkemade, Spectrochim. Acta, 28B, 289 (1973).
7. D. R. de Olivares, Ph. D. Thesis, Indiana University, Bloomington, IN (1976).
8. A. P. Baronavski and J. R. McDonald, J. Chem. Phys., 66, 3300 (1977).
9. A. C. Eckbreth, P. A. Bonczyk, and J. A. Shirley, "Investigation of Saturated Laser Fluorescence and CARS Spectroscopic Techniques for Combustion Diagnostics," EPA-600/778-104 (1978).
10. J. Kuhl, S. Neumann, and M. Kriese, Z. Naturforsch., A28, 273 (1973).
11. B. L. Sharp and A. Goldwasser, Spectrochim. Acta, 31B, 431 (1976).
12. B. W. Smith, J. D. Winefordner, and N. Omenetto, J. Appl. Phys., 48, 2676 (1977).
13. J. W. Daily and C. Chan, "Laser Induced Fluorescence Measurement of Sodium in Flames," presented at the Sixth International Colloquium on Gas Dynamics of Explosions and Reacting Systems, Stockholm, August, 1977.

14. G. D. Boutilier, M. B. Blackburn, J. M. Mermet, S. J. Weeks, H. Haraguchi, J. D. Winefornder, and N. Omenetto, Appl. Opt., 17, 2291 (1978).

15. N. Omenetto and J. D. Winefordner, "Atomic Fluorescence Spectroscopy with Laser Excitation," Chapter in Analytical Laser Spectrometry, N. Omenetto, ed., John Wiley, New Yor, (1978).

16. J. W. Daily, Appl. Opt., 17, 225 (1978).

17. A. C. Eckbreth, P. A. Bonczyk, and J. F. Verdieck, "Review of Laser Raman and Fluorescence Techniques for Practical Combustion Diagnostics," UTRC/R77-952665-6 (1977).

18. M. L. Pasons, B. W. Smith, and G. E. Bentley, Handbook of Flame Spectroscopy, p. 430, Plenum, New York (1975).

19. D. R. Jenkins, Proc. Roy. Soc., 293A, 493 (1966).

20. P. L. Lijnse and R. J. Elsenaar, J. Quant. Spectrosc. Radiat. Transfer, 12, 1115 (1972).

21. B. P. Kibble, G. Copley, and L. Krause, Phys. Rev., 159, 11 (1967).

22. H. P. Hooymayers and C. Th. J. Alkemade, J. Quant. Spectrosc. Radiat. Transfer, 6, 847 (1966).

23. C. Th. J. Alkemade and P. J. Th. Zeegers, "Excitation and De-Excitation Processes in Flames," chapter in Spectrochemical Methods of Analysis, J. D. Winefordner, ed., John Wiley, New York (1971).

24. W. L. Wiese, M. W. Smith, and B. M. Miles, Atomic Transition Probabilities, Vol. II, Sodium through Calcium, U. S. Government Printing Office, Washington, (1969).

25. P. J. Th. Zeegers, W. P. Townsend, and J. D. Winefordner, Spectrochim. Acta, 24B, 243 (1968).

26. H. Haraguchi, W. K. Fowler, D. J. Johson, and J. D. Winefordner, Spectrochim. Acta, 32A, 1539 (1976).

27. T. Tataczyk, E. H. Fink, and K. H. Becker, Chem. Phys. Lett., 40, 126 (1976).

28, H. G. C. Human and P. J. Th. Zeegers, Spectrochim. Acta, 30B, 203 (1975).

29. D. G. Jones and J. C. Mackie, Combustion and Flame, 27, 143 (1976).

30. J. VanderHurk, Th. Hollander, and C. Th. J. Alkemade, J. Quant. Spectrosc. Radiat. Transfer, 13, 273 (1973).

31. J. VanderHurk, Th. Hollander, and C. Th. J. Alkemade, J. Quant. Spectrosc. Radiat. Transfer, 14, 1167 (1974).

32. P. W. B. Pearce and A. G. Gaydon, The Identification of Molecular Spectra, 3rd Ed., Chapman and Hall, London (1965).

33. M. Ninomiya, J. Phys. Soc. Japan, 10, 829 (1955).

34. R. C. Johnson, Trans Roy. Soc., 226A, 157 (1927).

BIOGRAPHICAL SKETCH

Marlana Beth Blackburn was born in Austin, Texas, on April 19, 1951. She graduated in June, 1969, from H. B. Plant High School in Tampa, Florida. In March, 1973, she received the Bachelor of Science degree from the University of Florida, Gainesville, Florida. In September, 1974, she entered the University of Florida as a Graduate Student in the Department of Chemistry.

I certify that I have read this study and that in my opinion it conforms to acceptable standards of scholarly presentation and is fully adequate, in scope and quality, as a dissertation for the degree of Doctor of Philosophy.

James D. Winefordner

James D. Winefordner, Chairman
Graduate Research Professor of Chemistry

I certify that I have read this study and that in my opinion it conforms to acceptable standards of scholarly presentation and is fully adequate, in scope and quality, as a dissertation for the degree of Doctor of Philosophy.

Wallace S. Brey

Wallace S. Brey
Professor of Chemistry

I certify that I have read this study and that in my opinion it conforms to acceptable standards of scholarly presentation and is fully adequate, in scope and quality, as a dissertation for the degree of Doctor of Philosophy.

Hugh A. Moye

Hugh A. Moye
Associate Professor of Food Science and Human Nutrition

I certify that I have read this study and that in my opinion it conforms to acceptable standards of scholarly presentation and is fully adequate, in scope and quality, as a dissertation for the degree of Doctor of Philosophy.

Gerhard M. Schmid
Gerhard M. Schmid
Associate Professor of Chemistry

I certify that I have read this study and that in my opinion it conforms to acceptable standards of scholarly presentation and is fully adequate, in scope and quality, as a dissertation for the degree of Doctor of Philosophy.

William Weltner Jr
William Weltner, Jr.
Professor of Chemistry

This dissertation was submitted to the Graduate Faculty of the Department of Chemistry in the College of Liberal Arts and Sciences and to the Graduate Council, and was accepted as partial fulfillment of the requirements for the degree of Doctor of Philosophy.

December 1978

Dean, Graduate School